Advanced Optical Technologies

TYPE Original Research
PUBLISHED 07 January 2026
DOI 10.3389/aot.2025.1730807

OPEN ACCESS

EDITED BY
Manoj Kumar,
Kobe University, Japan

REVIEWED BY
Ben Urban,
Shimane University, Japan
Shiyu Zhang,
Beijing Information Science and Technology University, China

*CORRESPONDENCE
Zhengcong Du,
dzc38625686@126.com

RECEIVED 23 October 2025
REVISED 04 December 2025
ACCEPTED 08 December 2025
PUBLISHED 07 January 2026

CITATION
Li C, Wen L, Liu G, Du Z, Li J, Yang T and Jiao S (2026) PSO-based imaging restoration method for diffraction imaging systems.
Adv. Opt. Technol. 14:1730807.
doi: 10.3389/aot.2025.1730807

PSO-based imaging restoration method for diffraction imaging systems

Can Li[1,2], Lianghua Wen[2], Guochun Liu[1], Zhengcong Du[2]*, Jiaxun Li[2], Tong Yang[2,3] and Sanxiu Jiao[2]

[1]College of Aviation Engineering, Civil Aviation Flight University of China, Guanghan, China, [2]School of Electronic Information Engineering, Yibin University, Yibin, China, [3]School of Electronic Information Engineering, China West Normal University, Nanchong, China

Membrane diffraction imaging is one of the most widely used imaging technologies today, which offers the advantages such as lightweight design, large aperture, foldability, and low cost. However, the system imaging quality degrades because of the multiple order diffraction generated by the diffractive elements in practical applications. To eliminate the effects of multiple diffraction orders from the diffractive elements and optimize imaging quality, the system images are post processed. Iterative optimization algorithms are commonly used for image post processing. Particle swarm optimization is a commonly used iterative optimization algorithm, which is often used to search for optimal solutions within the solution space. The particle swarm optimization algorithm has the features of few parameters, simple behavior, and fast iteration speed, which can rapidly and effectively optimize imaging. This paper optimizes the simulated imaging of a diffraction imaging system based on Fresnel zone plates by adopting the particle swarm optimization algorithm. Optimize the system image based on known point spread functions and the system image. System imaging is optimized under the premise of known point spread functions and system imaging. The iteration speed is enhanced, reducing the number of iterations by approximately 99.6% compared to the random parallel gradient descent algorithm. Simultaneously, contrast is improved by about 5.4%, while gradient optimization effectiveness increases by approximately 25.4% after optimization by the particle swarm algorithm. Finally, the derived restoration model was applied to other images, achieving overall improvements in all evaluation metrics.

KEYWORDS

fresnel zone plate, imaging optimization, multiple orders diffraction, particle swarm optimization algorithm, point spread function

1 Introduction

The lightweight and high-resolution features of imaging systems have become a hot topic in the field of imaging development with the advancement of imaging technology. Membrane diffraction imaging was first proposed at the 1997 International Conference in Lure, France, which began to rapidly develop thereafter Chesnokov and Vasileisky (1997). This technology has been applied to space observation projects such as "Eyeglass", "GISMO", "MOIRE", and "Falcon-7", with a wealth of research findings and experience accumulated by relevant research institutions Hyde (1999), Hawarden

et al. (2004), Atcheson et al. (2014), Andersen et al. (2016). However, membrane diffraction imaging technology has not been widely adopted in practical applications, due to which the image quality is unable to meet the standards for spatial imaging in the imaging systems equipped with diffraction imaging elements Zhi et al. (2017), Jiang et al. (2020). Therefore, researchers from relevant institutions have conducted extensive research on diffraction imaging technology, such as optical system design Wang et al. (2002), Zhang et al. (2007), fabrication of binary optical elements Jian et al. (2016), Ruoqiu et al. (2017), system wavefront correction Wen et al. (2019), Zhu et al. (2019), and imaging optimization Yang et al. (2019), Yang et al. (2020). Image optimization is crucial for the practical application of subsequent imaging systems.

Recently, many research institutions have conducted extensive research on imaging optimization for diffraction imaging systems. Diffraction imaging systems based on Fresnel Zone Plates (FZP) are the most widely used in practical applications Bin et al. (2004), Wang et al. (2016). Optimizing the system image in diffraction systems differs significantly from traditional imaging systems. System image quality degrades due to multiple order diffraction generated due to the FZP's sub-structures. Simultaneously, image quality further deteriorates due to wavefront distortion affecting the beam during transmission through the system. To solve the problem of degraded image quality in diffraction imaging systems, various algorithms for imaging optimization have been proposed. Mainstream optimization methods include inverse filtering algorithms for different types of blur kernels Lu et al. (2019),Liang et al. (2021), blind deconvolution methods Fish et al. (1995), Fish et al. (2003), Krishnan and Fergus (2009), deep learning Kupyn et al. (2019), Hong et al. (2020), Zamir et al. (2021), and model-based enhancement methods Lianghua et al. (2017), Lianghua et al. (2018). However, image optimization methods based on the FZP diffraction imaging model have been rarely reported in recent years, and the related research has primarily focused on algorithms with complex behaviors, which leads to inefficient optimization iterations. Between 2024 and 2025, Li Jiaxun et al. conducted further research for imaging models. The Stochastic Parallel Gradient Descent (SPGD) algorithm, Simulated Annealing (SA), and Cuckoo Search algorithm are combined with imaging models. The PSF and the numerical solution of the optimized image are input to the imaging model, which optimizes the image of the imaging syste Wen et al. (2024), Li et al. (2025).

The paper is organized as follows: In Section 2, a diffraction imaging system based on FZP was simulated using optical simulation software. Image data was obtained through this system, and an imaging model was derived based on the imaging characteristics of FZP. Subsequently, in Section 3, an image optimization algorithm based on particle swarm optimization (PSO) was established in combination with the imaging model. The image was iteratively optimized, and the optimization results were analyzed. In Section 4, the results of the PSO iterative optimization were input into the imaging model to rapidly restore the image, and the rapid optimization results were analyzed. In Section 5, conclusions were drawn, and plans for future work were outlined.

2 Imaging system and model

This section provides research on the simulation and imaging model of the FZP diffraction system. The FZP-based diffraction imaging system is simulated and analyzed using optical simulation software. The system analysis includes the modulation transfer function (MTF), wavefront, point spread function (PSF), spot diagram, and extended target imaging, which can determine the system image performance and the accuracy of extended target imaging data, to ensure the effectiveness of image optimization. Subsequently, the imaging model of the imaging system is established based on the imaging characteristics of the FZP imaging system to solve for the optimized image.

2.1 FZP imaging principle

System simulation of the optical imaging model was conducted. An 800 mm-aperture FZP diffraction imaging system was constructed using simulation software. The imaging system comprised two FZP elements, three double bonded lenses, and a filter. The parameters of each element in the system are used as design parameters for the FZP diffraction imaging system, which include the radius of curvature, effective aperture, distance between optical surfaces, and corresponding materials. The FZP is parameterized. Simulation of the FZP is achieved by combining a binary surface with a standard optical surface. The setting of the binary surface requires not only setting the basic surface parameters but also setting the corresponding phase coefficients. The phase coefficient is determined by Equation 1.

$$\phi = M\sum_{i=1}^{N} a_i \rho^{2i} \tag{1}$$

Where ϕ denotes the phase of the optical surface, M denotes the diffraction order used by the optical surface, N corresponds to the index of the polynomial coefficient in the order, and a_i is the coefficient of the 2i-th power of ρ (the phase coefficient). The phase coefficients a_1 to a_5 are to be set, and the phase coefficients are obtained by setting the optimization function with respect to the system wavefront aberration and the system focal length. Finally, quartz was selected as the substrate material for FZP, which determined all parameters of the FZP.

Subsequently, the double bond lens is designed and calculated in the system. Unlike traditional lens calculations, the radius of curvature for a double bond lens is calculated by selecting material combinations. The combination of crown glass in front and flint glass in back is commonly used in double bond lens design. Material refractive indices are obtained by searching the corresponding combinations. Parameters are substituted into equations Equations 2–4 to determine the optical surface curvature, which includes the radius of curvature, refractive index, focal length, and other parameters.

$$\varphi = \frac{1}{f} \tag{2}$$

$$\varphi_1 = (n_1 - 1) * \left(\frac{1}{r_1} - \frac{1}{r_2}\right) \tag{3}$$

10.3389/aot.2025.1730807

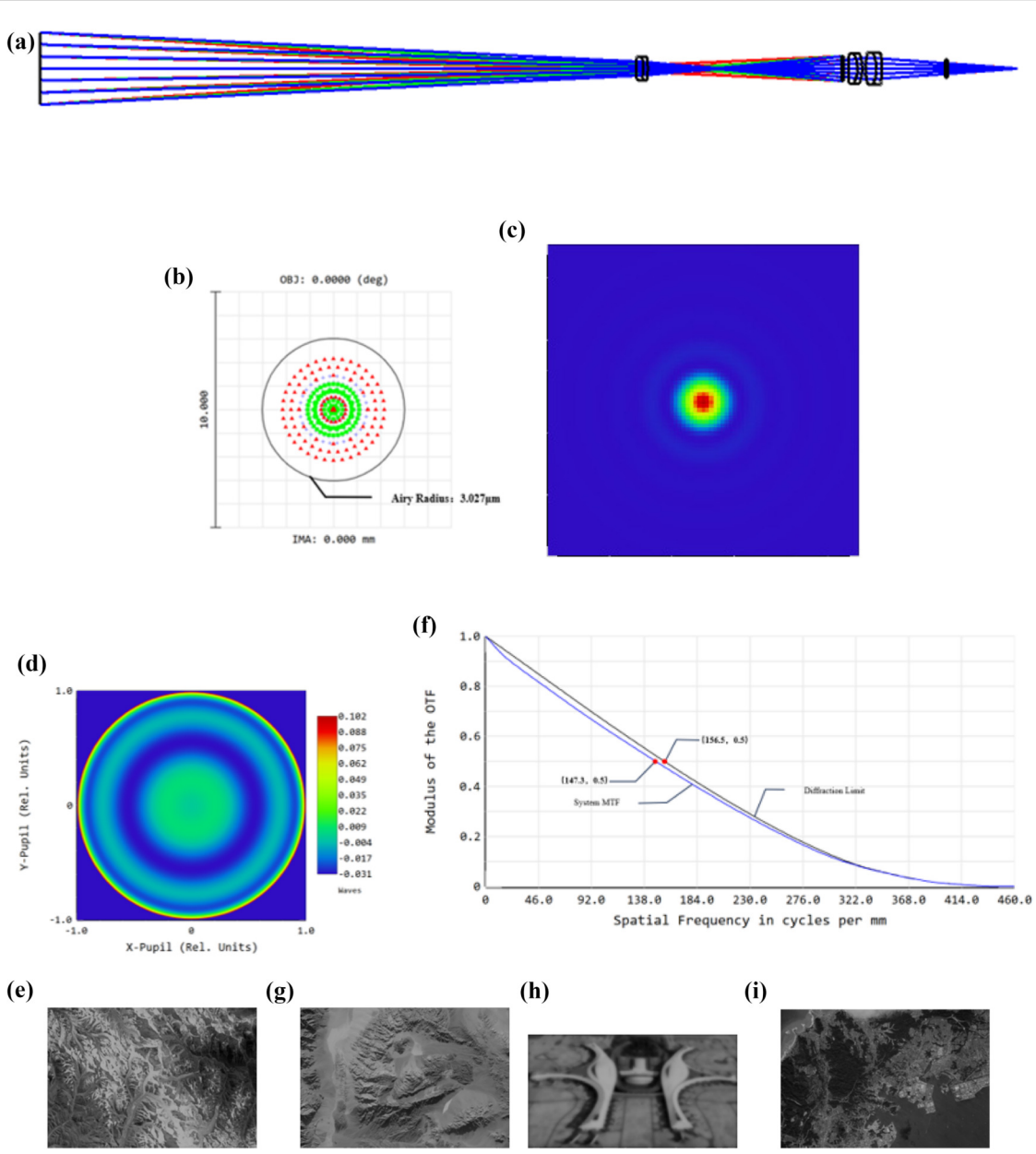

FIGURE 1
FZP imaging model and imaging performance. **(A)** FZP imaging system; **(B)** spot diagram; **(C)** PSF; **(D)** wavefront; **(E)** MTF; **(F–I)** extended target imaging.

$$\varphi_2 = (n_2 - 1) * \left(\frac{1}{r_2} - \frac{1}{r_3}\right) \tag{4}$$

Where φ represents the optical power between adjacent optical surfaces, which is inversely proportional to the focal length f. Among them, φ_1 represents the optical power from the first optical surface to the second optical surface, and φ_2 represents the optical power from the second optical surface to the third optical surface. n represents the refractive index between adjacent optical surfaces. r is the radius of curvature of each optical surface.

The FZP imaging system, as shown in Figure 1a, is analyzed in terms of its imaging model. The analysis of the imaging model primarily involves the analysis of point target imaging and extended target imaging, such as the imaging system's PSF, spot diagram, wavefront, MTF, and extended target imaging analysis.

As shown in Figure 1b, the inconsistent sizes of light spots focused at different wavelengths on the same image plane, which shows that chromatic aberration still exists in the system. Moreover, chromatic aberration causes image quality degradation.

As shown in Figure 1c, the PSF exhibits no distortion, the energy is concentrated, and the Airy disk size is 3.027 μm, which shows the system has excellent focusing performance.

In the wavefront Figure 1d, the wave trough is approximately −0.031 wavelengths, and the wave crest is

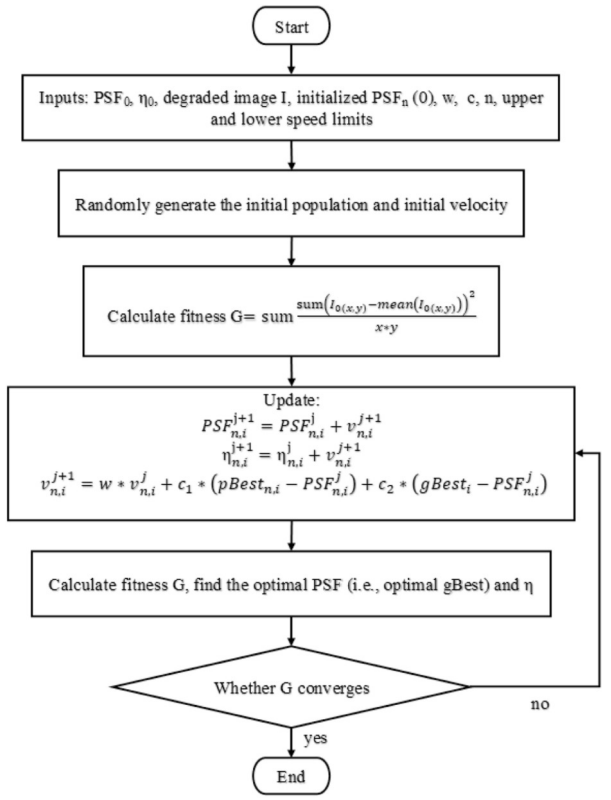

FIGURE 2
The optimization flow of imaging model parameters within PSO algorithm.

approximately 0.102 wavelengths. The wavefront aberration was calculated to be 0.132 wavelengths, which is less than one-quarter wavelength. This result is consistent with the Rayleigh criterion, which indicates that although wavefront distortion exists in the system, but wavefront distortion has little effect on imaging, which indicates the system image quality is good.

In Figure 1e, the optical transfer function (OTF) approaches zero when the spatial frequency reaches 414 cycles/mm. The system MTF closely matches the diffraction-limited MTF curve, which indicates that the system's transmission capability approaches that of an ideal imaging system. However, the mid-frequency component of the system MTF differs by 9.2 cycles/mm from the diffraction-limited mid-frequency component, which indicates the presence of aberrations within the system. System chromatic aberration leads to reduced imaging quality.

After completing the point target imaging analysis, the extended target imaging is analyzed at 550 nm primary wavelength. The extended target imaging plane sampling is set to 1024 × 1024. The single-wavelength imaging is acquired as shown in Figures 1f–i. In the extended target imaging, the image exhibits not distortion, but the imaging has the problem of edge blurring and loss of imaging details. Combined with PSF analysis, the imaging blur was attributed to multiple order diffraction from the diffractive elements. To address the imaging blur issue, the imaging model was derived based on the imaging characteristics of the FZP.

2.2 Imaging model

During the process of imaging optimization research, the imaging model is established for the system, which is used for subsequent further development of imaging optimization studies. In 2023, Li Jiaxun et al. proposed an imaging restoration method based on the FZP imaging model, performing mathematical derivations for the FZP diffraction imaging system. An imaging model for an FZP imaging system was derived, with the expression shown in Equation 5; Li et al. (2023).

$$I = I_0 * [PSF_1 \times \eta_1 + PSF_n \times (1 - \eta_1)] \tag{5}$$

Where I denotes the extended target image directly obtained by the FZP imaging system, and I_0 denotes the optimized result of the extended target image from the FZP system. η_1 and PSF_1 represent the diffraction efficiency and point spread function (PSF) of the designed imaging order, respectively. PSF_n denotes the effective point spread function of stray light and noise in the imaging system. The imaging model is represented by the interaction between the designed-order light and scattered light and noise, where the designed-order light is expressed as $I_0 * (PSF_1 \times \eta_1)$, and the non-designed-order light and noise are expressed as $I_0 * [PSF_n \times (1 - \eta_1)]$.

However, Equation 5 cannot directly solve for numerical solutions, which only solves the analytical solutions in practical applications. Meanwhile, analytical solutions cannot intuitively reflect imaging effects. To solve the problem, data is input into imaging models for specific calculations. However, the imaging quality collected by the system cannot meet the requirements for direct solutions. Therefore, to solve the problem of degraded imaging quality, the input image is optimized. Optimizing the image actually constitutes a multi-objective optimization problem, which can be summarized as a multi-objective optimization expression, as shown in Equation 6.

$$\begin{aligned} &\max(\text{or}\min)(f(x)) = \{f_1(x), f_2(x), \ldots, f_n(x)\} \\ &\text{s.t}\, x \in \Omega \end{aligned} \tag{6}$$

Where $f(x)$ usually is the evaluation function of the optimization objective, which is also called the objective space. Meanwhile, Ω is the space where $(x_1, x_2, \ldots, x_n)$ is located, which is called the decision space. For multi-objective optimization problems related to image optimization, image metrics are usually selected as evaluation functions. By combining the imaging model, the imaging of the FZP imaging system is converted into a mathematical expression, and the iterative optimization problem related to the image is converted into a multi-objective optimization problem. The expression is shown in Equation 7.

$$\begin{aligned} &Z = \max(f(PSF)) = \{f_1(PSF), f_2(PSF), \ldots, f_n(PSF)\} \\ &\text{s.t}\, PSF \in \Omega \end{aligned} \tag{7}$$

Where image gradient and contrast are selected as optimization metrics. Parameters are adjusted while changes in gradient and contrast are observed throughout the optimization process. The decision space is populated through iterative updates, while the decision space values are continuously input to the target space. The Z-value is calculated, which corresponds to the PSF value in the decision space representing the optimized result. Finally, the

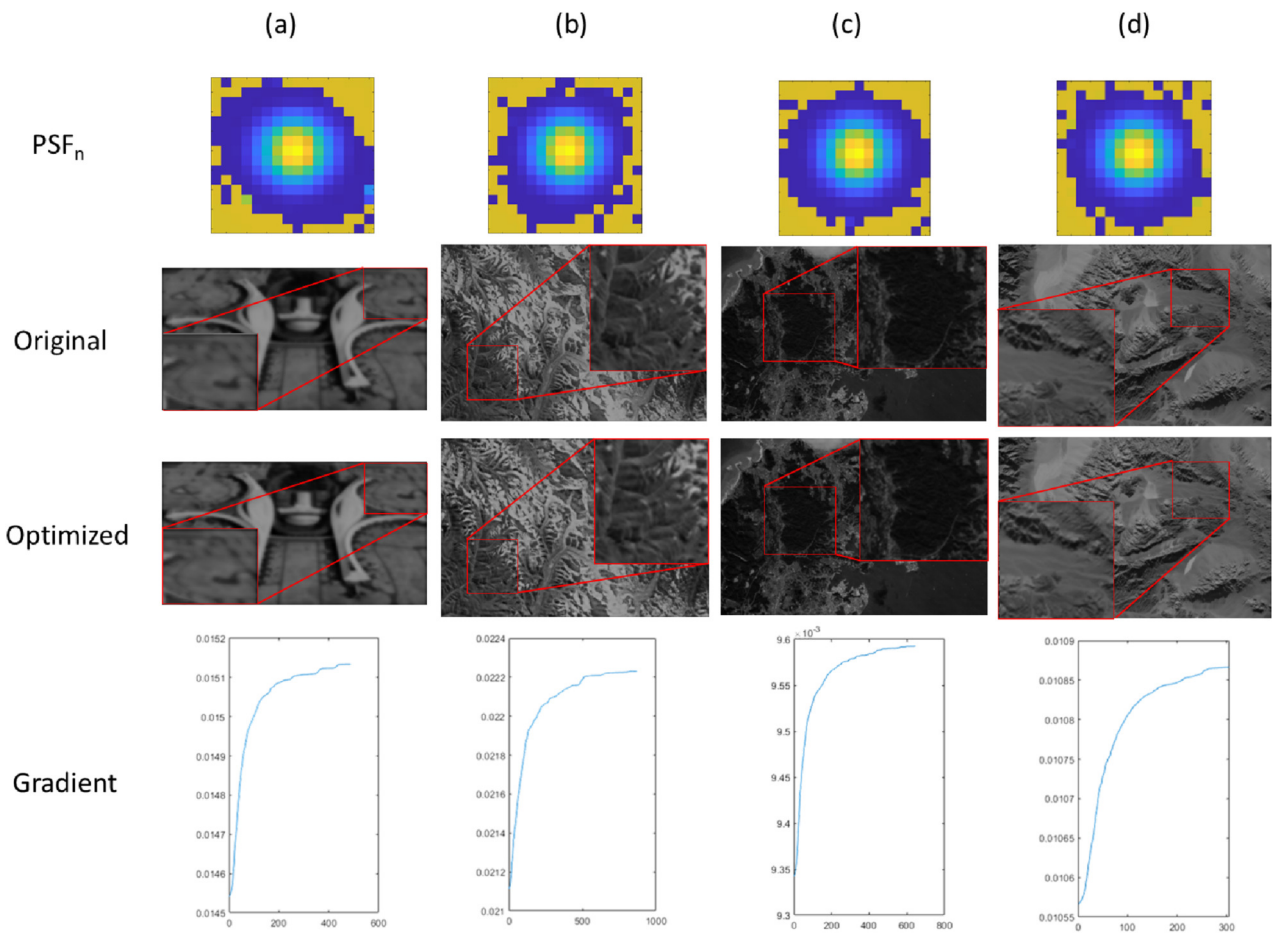

FIGURE 3
PSO optimization iterative results.

optimized PSF is input to the imaging model to obtain the iteratively optimized image I.

However, some problems still exist in the specific research of PSF iterative optimization. Optimization algorithms such as Stochastic Parallel Gradient Descent (SPGD), Simulated Annealing (SA), and Cuckoo Search are applied to imaging optimization, which have some drawbacks including high iteration counts, slow iteration speeds, numerous parameters, and suboptimal optimization results. PSO effectively addresses these issues due to its simple behavior, fast iteration speed, and minimal parameter requirements.

3 Optimized solution of FZP imaging model

The PSO algorithm is an evolutionary computation technique that was developed by Kennedy and Eberhart (1995). The algorithm achieves global optimization through collaboration and competition among particles, which features in practice, including few parameters, simple behavior, and fast iteration speed Liping and Zhang (2003). By integrating with imaging models, the PSO algorithm can solve for numerical solutions to imaging models, which can effectively address the degradation of imaging quality caused by multiple-order diffraction. Simultaneously, PSO can simplify the optimization process, which can greatly reduce the time required for iterative optimization, thereby improving optimization efficiency.

3.1 PSO algorithm principle

The particle swarm optimization achieves global search optimization primarily through collaboration and competition among individuals. First, a group of random solutions must be generated through initialization, which are equivalently regarded as particles that have no mass or volume. Global optimization is completed by particles flying in the search space. This flight pattern references the flying behavior of flocks of birds or the foraging behavior of schools of fish, and the behavior function is shown in Equation 8.

$$x_i^{(j+1)} = x_i^j + v_i^{(j+1)} \tag{8}$$

The PSO iteration method is simple: particles move based on the velocity generated by weighting their current positions, and the

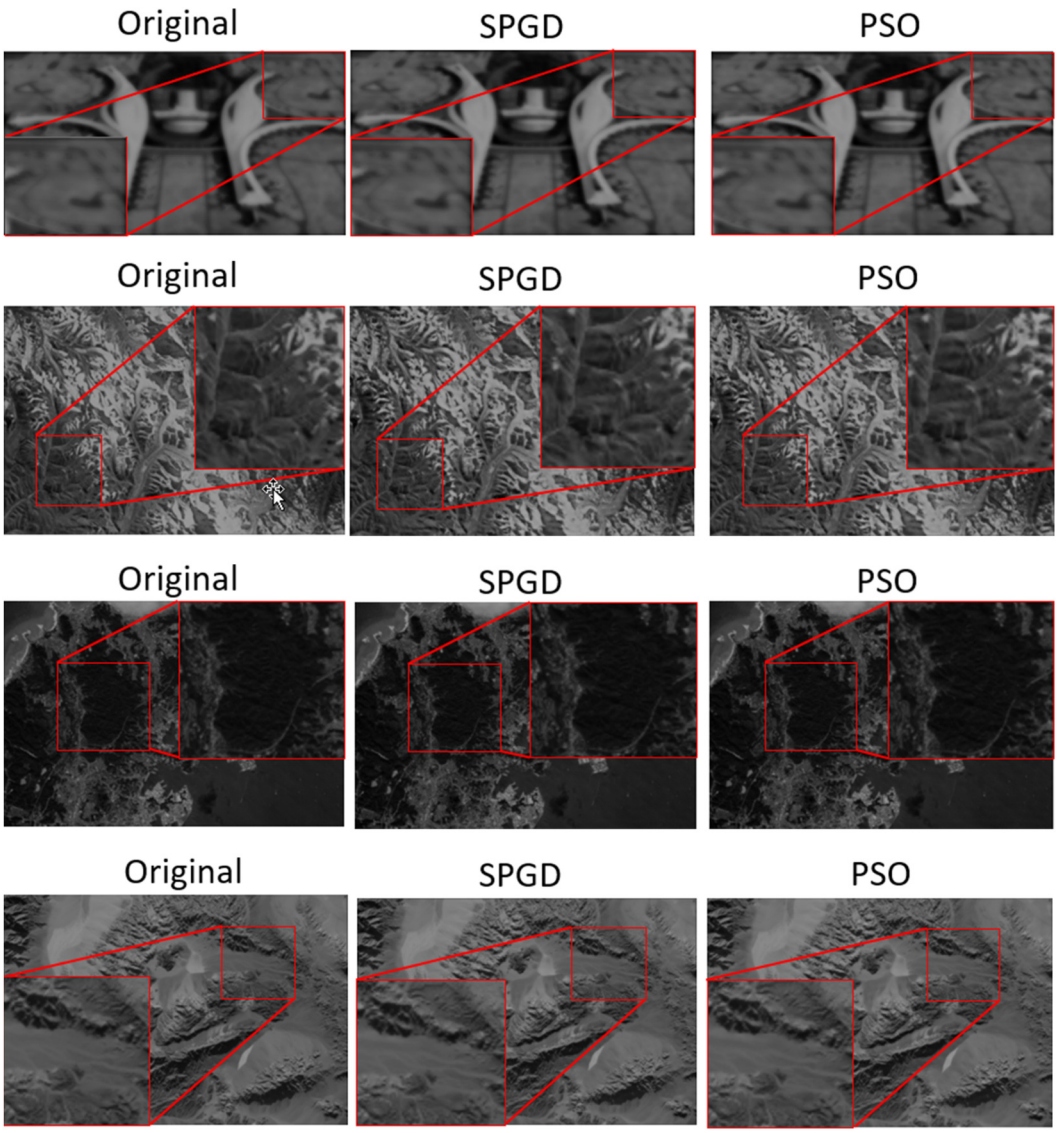

FIGURE 4
Comparison of optimization results between PSO and SPGD.

TABLE 1 Iterative optimization comparison.

Image	Algorithm	Contrast	Gradient	MAE	NMSE	Number of iterative
(a)	SPGD	9271.9/9303.8	0.0145/0.015	15.8582	2.6510e-04	215395
	PSO	9280/9314	0.0145/0.0151	21.1207	4.6841e-04	488
(b)	SPGD	9827.5/10279	0.0211/0.022	54.2139	0.0027	94595
	PSO	9908.1/10388	0.0211/0.0222	64.3485	0.0038	871
(c)	SPGD	9217.9/9241.7	0.0093/0.0095	12.5631	4.1329e-04	243360
	PSO	9223.1/9247.2	0.0093/0.0096	15.2258	6.0790e-04	646
(d)	SPGD	7878.2/7960.5	0.0106/0.0108	21.2138	4.4073e-04	230533
	PSO	7896.8/7986.7	0.0106/0.0109	26.7475	6.9743e-04	305

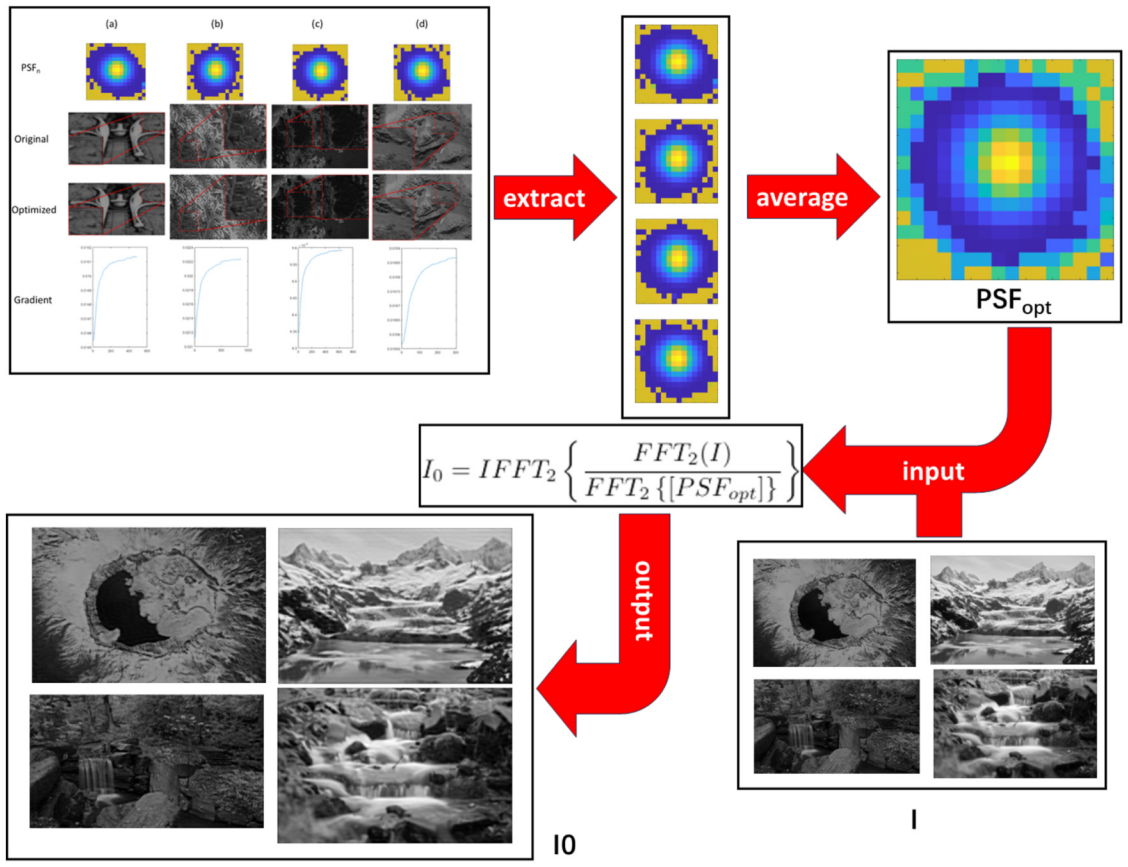

FIGURE 5
Fast image restoration based on PSO.

velocity is continuously updated during the iteration process. The iteration formula for velocity is shown in Equation 9.

$$v_i^{j+1} = \omega \times v_i^j + c_1 \times rand\,(nd, nd) \times \left(\text{pbest}_i - x_i^j\right) + c_2 \times rand\,(nd, nd) \times \left(\text{gbest}_i - x_i^j\right) \quad (9)$$

Equation 9 is primarily used to update the velocity of particles in each movement within the PSO. The velocity iteration formula includes a memory term, an individual learning term, and a social learning term. Where ω is the inertia factor, which is required to be non-negative and it can be used to adjust the strength of the algorithm's optimization capability. c is the learning factor, where c_1 is the cognitive learning factor, c_2 is the social learning factor. The learning factor can effectively adjust the search capability of the algorithm. Where nd represents the matrix size. where pbest denotes the local optimum of the particle swarm, which is the optimal population. Gbest denotes the global optimum of the particle swarm, which is the optimal particle. During velocity iteration, the first memory term is used to relate the previous generation's velocity to the post-iteration velocity, because the velocity itself has no memory. If the memory term is absent, the iterative optimization process assumes that a particle at the globally optimal position remains stationary, while other particles move toward a weighted center between the individual optimal and global optimal positions. In this case, the optimal particle will only be found at the current best position. To induce particle movement and achieve global optimization, the inertia weight is added to the memory term. The inertia weight originates from the concept proposed by Clerc, which uses a decay factor to ensure algorithm convergence. However, subsequent research discovered that setting a maximum velocity limit can enhance algorithm performance. This method eliminates the link between the inertia factor and the learning factor, which ensures the effectiveness and independence of the memory term Clerc (1999). The second term represents the individual cognitive component, which indicates the particle's own thinking, providing iterative particles with powerful global search capabilities and avoiding local minimal. Finally, the third term is the population cognitive component, embodying information sharing among particles. The PSO's optimization is effectively achieved through the synergistic interaction of these three components.

Before the iteration begins, the input population, velocity, and optimal population must be initialized. To accommodate optimization requirements, each particle in the solution space is two dimensional data, which needs to be fitted. The input

population, velocity, and initialized optimal population must be converted into two dimensional matrices. The initialization formula is shown in Equation 10.

$$v_i = DL. * ones(nd, nd) + [UL. * ones(nd, nd) - DL. * ones(nd, nd)]. * 0.01. * [rand(nd, nd)] \quad (10)$$

Where DL denotes the minimum value of a single pixel in the matrix, and UL denotes the maximum value. 'ones ()' is used to generate a matrix with all values set to 1, while 'rand ()' is used to generate a random matrix.

After outputting the new velocity, the particle update iteration is achieved: the new velocity is input into the PSO particle update behavior, which makes the particle move. Subsequently, the output particle swarm is evaluated. The gradient of the expanded target image is selected as the criterion for algorithm termination, which is also used as the judgment condition for iterative optimization. The calculation expression is shown in Equation 11.

$$G = \left[I(x, y) - \frac{1}{M \times N} \sum_{x=1,y=1}^{M,N} I(x, y) \right]^2 \Big/ (M \times N) \quad (11)$$

Where I (x, y) is the restored image obtained through a single iteration of the optimization algorithm, (x, y) denotes the pixel coordinates in the Cartesian coordinate system, and M and N respectively represent the dimensions of the image.

Based on the above calculations, the operation flow of the PSO-based image optimization algorithm is shown in Figure 2.

In the optimization process of the target image, initial parameters are firstly input. The upper and lower limits are determined by collecting the maximum and minimum values of the PSF in the simulation system. Because of the simulation model operating under ideal conditions, the background noise of collected images is not considered in the input PSF and target image expansion process. After the initial parameters are input, the initial velocity and a random population are generated. The generated random population and random velocities are input to the evaluation function. The gradient and contrast are calculated, which are compared with the next-generation's results. Subsequently, the corresponding parameters are input to the PSO for iterative optimization. Firstly, the velocity values for the next particle movement are calculated in the optimization process. Subsequently, the output velocity values are input to the particle movement behavior, and a new particle swarm is obtained. The new particle swarm is input to the evaluation function for assessment, which results in corresponding image metrics. Finally, the image metrics are evaluated to determine whether convergence conditions are met, thereby deciding whether to terminate the algorithm.

3.2 Algorithm simulation and analysis

This paper combines imaging models with the PSO algorithm to propose a PSO-based image optimization method. This approach logically simplifies the optimization iteration process, thereby reducing iteration time, and improving iterative optimization efficiency. To further validate the theoretical effectiveness, the expanded target image from the imaging model is input into the PSO-based optimization algorithm.

Randomly generated PSFs are treated as particles in the iterative optimization process, while PSFs and extended target images collected from the FZP system image model are input to the PSO optimization algorithm. Subsequently, PSO initial parameters are set, including the population size, upper and lower velocity bounds, filtering radius, learning factor, and inertia factor. The parameters are configured and adjusted, which ensures stable algorithm operation. Subsequently, to evaluate optimization effectiveness, the image gradient G is selected to assess convergence of the optimization iterations and serves as the algorithm's termination condition. The algorithm then stops automatically upon meeting the specified optimization conditions. The corresponding pseudocode is shown in Algorithm 1.

Input: The inertia factor ω, the diffraction efficiency η_0, the learning factors c_1 and c_2, the image size M and N, filter radius R, minimum value DL and maximum value UL, and number of population n

Output: *gbest*

Initialize particle swarm $x(:,:,i) = \{x_1, x_2, \ldots, x_n\}$, velocity $v(:,:,i) = \{v_1, v_2, \ldots, v_n\}$, and $pbest(:,:,i) = \{pbest_1, pbest_2, \ldots, pbest_n\}$ by Equation 12
for $i = \{1, 2, \ldots, n\}$ **do**
  Calculate the gradient G(x) and G (pbest) (Equation 11)
end for
while (G (gbest) is convergent) **do**
  if G(x) > G (pbest) **then**
    pbest = x
  else
    pbest = pbest
  end if
  G (gbest) = Max (G (pbest (:, :, i))) ⇒ gbest
  for $i = \{1, 2, \ldots, n\}$ **do**
    Update the speed value $v^{(j+1)}(:,:,i)$ (Equation 9)
    Update the particle swarm $x^{(j+1)}(:,:,i)$ (Equation 8)
    if G(x) > G (pbest) **then**
      pbest = x
    else
      pbest = pbest
    end if
  end for
  G (gbest) = Max (G (pbest (:, :, i))) ⇒ gbest
  if (Find (G (gbest) = Max (G (gbest))) ≥ 50) **then**
    Break
  end if
end while

Algorithm 1. Procedure of PSO algorithm.

Where the diffraction efficiency η_0 is calculated through the simulation system. The inertia factor is set to a small value, which

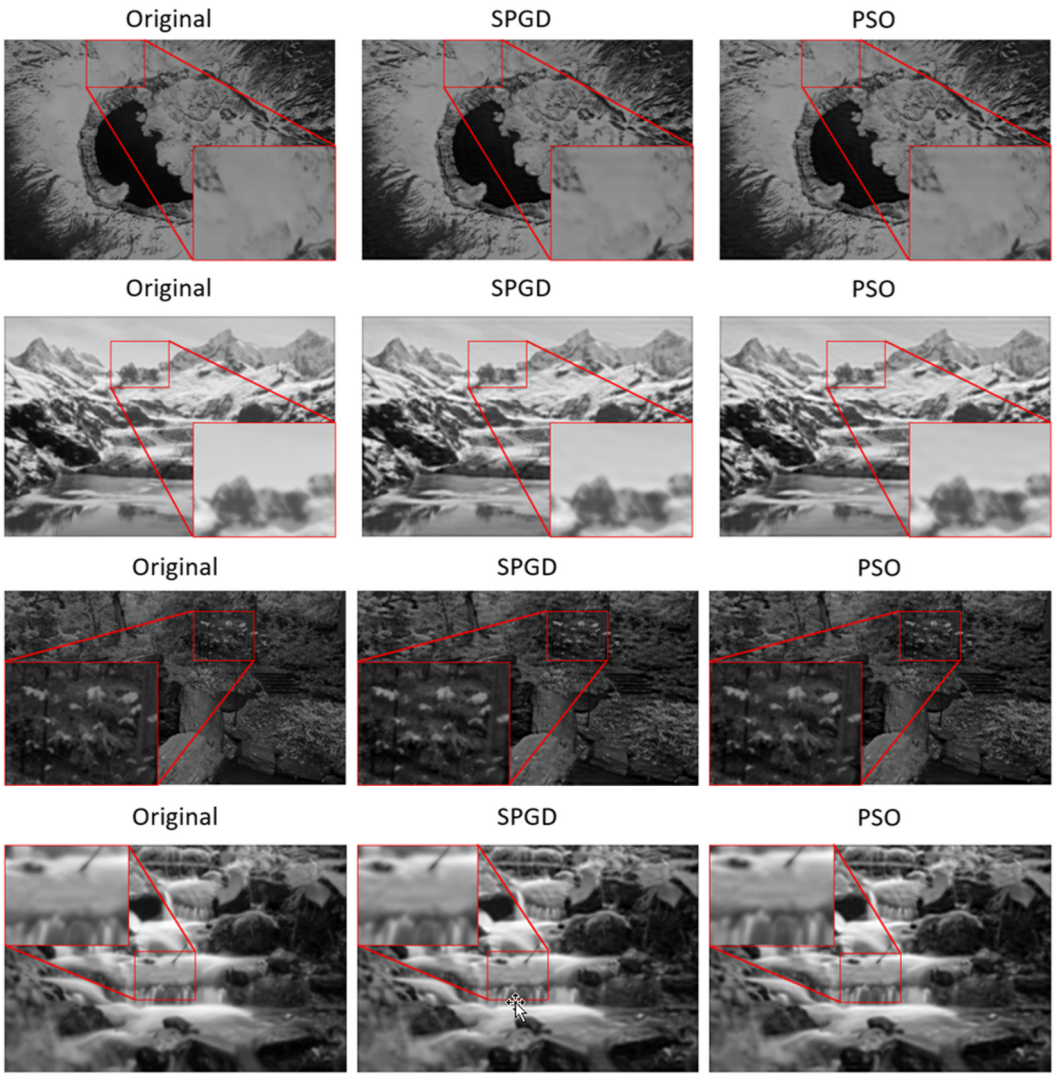

FIGURE 6
Comparison of restoration between PSO and SPGD.

ensures the accuracy of optimization by reducing the influence of the previous generation's particle positions on the next-generation. The cognitive learning factor c_1 and the social learning factor c_2 are set to the same value, which balances local and global optimization capabilities. After inputting the corresponding parameters, optimization results are obtained through continuous iterative optimization until the algorithm terminates. Unlike traditional PSO algorithms, the termination condition is explicitly defined, because the PSO applied to image optimization cannot complete optimization within a determined number of iterations. so, the termination condition is set: the algorithm stops when the image gradient G ceases to increase over a period of time.

At every iteration, the updated PSF, the PSF of the imaging system under consideration, and the expanded target image are input to the imaging model for computation, which results in the corresponding optimized image. The results including the PSF_n after optimization iterative, images before and after optimization, and the gradient enhancement curve of the optimization iteration. The relevant optimization results are shown in Figure 3.

As shown in Figure 3, four images are optimized through iterative processing, which results in enhanced imaging details and improved image resolution. The result confirms the feasibility of the PSO algorithm in image restoration.

The comparative analysis of SPGD optimization results and PSO optimization results, to systematically evaluate PSO's image optimization capabilities and mitigate algorithmic randomness and chance effects. The optimization results comparison is shown in Figure 4.

By comparing the optimization results of the PSO and SPGD algorithms, the PSO-optimized images have richer and clearer details compared to those optimized by SPGD.

To quantitatively evaluate the optimization performance of both algorithms, the contrast, gradient, and number of iterations for each algorithm were compared, which further validates the feasibility of PSO for system image optimization. The iterative optimization comparison is shown in Table 1.

The relevant metrics for iterative optimization between the two methods were compared, which include contrast, gradient,

TABLE 2 Restoration comparison.

Image	Algorithm	Contrast	Gradient	MAE	NMSE
(a)	SPGD	9950.4/10143	0.0273/0.0276	34.1911	8.3463e-04
	PSO	9950.4/10207	0.0273/0.0276	43.6508	0.0014
(b)	SPGD	1049.8/1218.7	0.0518/0.0523	32.0392	9.1840e-04
	PSO	1049.8/1270.9	0.0518/0.0518	40.4641	0.0015
(c)	SPGD	11356/11559	0.0121/0.0125	36.7806	0.0028
	PSO	11356/11646	0.0121/0.0126	48.9242	0.0050
(d)	SPGD	392.6525/482.6343	0.0484/0.0487	23.7830	9.2797e-04
	PSO	392.6525/510.3621	0.0484/0.0486	39.9106	0.0015

mean absolute error, normalized mean square error, and number of iterations. The relevant data from the iterative optimization of both methods were compared, leading to the conclusion: PSO achieves superior iterative optimization results for images, requiring fewer iterations and demonstrating higher optimization efficiency. PSO algorithm is particularly suitable for diffraction imaging systems based on FZP was further demonstrated.

4 Restoration imaging base on model

After completing the iterative optimization of the image, to accelerate the optimization speed, the imaging model is transformed, and a fast restoration model is derived. Subsequently, the iterative optimization results are extracted and processed. The processed results are input to the fast restoration model, which performs rapid image restoration. Finally, the SPGD iterative optimization results are processed and input to the fast restoration model. By comparing the fast recovery results from both algorithms, the feasibility of the fast restoration method is confirmed.

4.1 Restoration simulation

To obtain a fast restoration model, the imaging model is derived. First, the imaging model equation is transformed using a two-dimensional Fourier transform on both sides, obtaining the expression shown in Equation 12.

$$FFT_2(I) = FFT_2(I_0) \times FFT_2\{[PSF_1 \times \eta_1 + PSF_n \times (1-\eta_1)]\} \tag{12}$$

Where FFT_2 denotes the two-dimensional Fourier transform. If the data for PSF_n, η_1, and PSF_1 can be obtained, images acquired by the FZP imaging system can be rapidly reconstructed. The analytical expression for the optimized image is derived through formula manipulation, as shown in Equation 13.

$$I_0 = IFFT_2\left\{\frac{FFT_2(I)}{FFT_2\{PSF_{opt}\}}\right\} \tag{13}$$

The $IFFT_2$ denotes the two-dimensional inverse Fourier transform. The analytical solutions for the imaging model parameters PSF_n, η_1, and PSF_1 are derived through analytical methods, which are substituted into Equation 13 to obtain the optimized image. This paper obtains the optimal numerical solution by using the particle swarm optimization algorithm, which achieves image optimization. The workflow is shown in Figure 5.

To achieve fast restoration of acquired images, PSF_n for different images is extracted after PSO optimization iterations. PSF_{opt} is obtained by averaging multiple PSF_n. Subsequently, PSF_{opt} and other images are input into the fast restoration model for reconstruction, which completes the PSO-based fast image reconstruction method.

4.2 Analysis

To further evaluate the optimization performance of the PSO algorithm, while avoiding the randomness and unpredictability of reconstruction, the reconstruction results from PSO-based imaging were compared with those from SPGD. Since fast reconstruction without iteration, the comparative analysis primarily included the image details, image gradients, and image resolution of the extended target imaging.

Restored images based on the PSO algorithm and SPGD algorithm are obtained through fast optimization. Comparison of the two algorithms is used to validate the feasibility and accuracy of the fast optimization. The comparison of the fast-restored images is shown in Figure 6.

Four images are selected for comparison, and when compared with the original images, the conclusion is reached: The PSF_{opt} obtained through iterations of both algorithms is input to the fast restoration model. The optimized images are locally enlarged and compared, which reveals that the fast-optimized images exhibit increased imaging details and improved image resolution. However, compared to the SPGD algorithm, the restoration results obtained by PSO iteration when PSF_{opt} is input into the imaging model output demonstrate superior performance. However, the comparison of images cannot quantitatively describe the restoration effect. Therefore, the restoration metrics of SPGD and PSO are compared with the original image metrics, as shown in Table 2.

Through the comparison, the conclusion that PSO achieves superior optimization results in imaging is verified. PSO optimizes image contrast and gradient more effectively. In the optimization of extended target imaging, PSO significantly enhances image detail compared to SPGD optimization. Consequently, the conclusion can be reached that PSO effectively optimizes imaging with superior results.

5 Conclusion

The multiple levels of FZP diffraction imaging system are simulated and analyzed. Subsequently, the PSO optimization algorithm was established, which combines the imaging model with the principle of PSO iterative optimization. The extended target image are input to PSO, the output images of iterative optimization are obtained. The optimized PSF_n is extracted from the iterative optimization results. The average PSF across multiple images is calculated as PSF_{opt} and input to the fast restoration model, which is used to achieve rapid optimization for other extended target images. The test results demonstrate: the restored diffraction images exhibit enhanced contrast, gradient, and other aspects. The output images are compared with SPGD optimization for diffraction imaging systems, concluding that PSO achieves superior optimization effects for the system image with higher efficiency.

The paper aims to validate the feasibility of full simulation for diffraction imaging systems. The images are optimized combining the PSO optimization algorithm, which is derived from the FZP diffraction imaging system. Subsequent research will focus primarily on wavefront correction for adaptive optics systems. The optical platform is planned to be constructed to verify the practical applicability of the FZP diffraction imaging system.

Data availability statement

The original contributions presented in the study are included in the article/supplementary material, further inquiries can be directed to the corresponding author.

Author contributions

CL: Validation, Methodology, Writing – review and editing, Formal Analysis, Conceptualization, Data curation, Investigation, Software, Writing – original draft, Visualization. LW: Project administration, Methodology, Formal Analysis, Data curation, Supervision, Writing – review and editing, Funding acquisition, Conceptualization, Software, Resources. GL: Methodology, Supervision, Writing – review and editing, Data curation, Conceptualization. ZD: Data curation, Resources, Project administration, Writing – review and editing, Supervision, Funding acquisition. JL: Methodology, Formal Analysis, Supervision, Writing – review and editing, Visualization. TY: Writing – review and editing, Investigation, Formal Analysis. SJ: Writing – review and editing.

Funding

The author(s) declared that financial support was received for this work and/or its publication. This work was supported by Sichuan Science and Technology Program under Grant NO. 2024ZYD026 and National Natural Science Foundation of China under Grant No.61975171.

Acknowledgements

We extend our appreciation to our colleagues for their constructive discussions and valuable suggestions, which have greatly enriched the quality of this work.

Conflict of interest

The author(s) declared that this work was conducted in the absence of any commercial or financial relationships that could be construed as a potential conflict of interest.

Generative AI statement

The author(s) declared that generative AI was not used in the creation of this manuscript.

Any alternative text (alt text) provided alongside figures in this article has been generated by Frontiers with the support of artificial intelligence and reasonable efforts have been made to ensure accuracy, including review by the authors wherever possible. If you identify any issues, please contact us.

Publisher's note

References

Andersen, G., Asmolova, O., McHarg, M. G., Quiller, T., and Maldonado, C. (2016). FalconSAT-7: a membrane space solar telescope. *Space Telesc. Instrum. 2016 Opt. Infrared, Millim. Wave. July.* 9904, 574–581. doi:10.1117/12.2229711

Atcheson, P., Domber, J., Whiteaker, K., Britten, J. A., Dixit, S. N., and Farmer, B. (2014). MOIRE: ground demonstration of a large aperture diffractive transmissive telescope. *Space Telesc. Instrum. 2014 Opt. Infrared, Millim. Wave. August* 5487, 535–549. doi:10.1117/12.2054104

Bin, Z., Ming, W., Shouping, N., and Suqing, T. (2004). Design and fabrication of fresnel zone plates. *Laser J. January.* 24, 20–21. doi:10.3969/j.issn.0253-2743.2003.01.007

Chesnokov, Y. M., and Vasileisky, A. S. (1997). "Space-based very high resolution telescope based on amplitude zoned plate," in *Paper presented at the international conference on space optics*. Toulouse, France.

Clerc, M. (1999). 3. June, 1951–1957. doi:10.1109/CEC.1999.785513

Fish, D., Brinicombe, A., Pike, E., and Walker, J. (1995). Blind deconvolution by means of the richardson–lucy algorithm. *J. Opt. Soc. Am. A* 12, 58–65. doi:10.1364/josaa.12.000058

Fish, D., Brinicombe, A., Pike, E., and Walker, J. (2003). Development of blind image deconvolution and its applications. *J. X-ray Sci. Technol.* 11, 13–19. doi:10.3233/xst-2003-00065

Hawarden, T. G., Cliffe, M. C., Henry, D. M., Stevens, J. A., and Greve, T. (2004). Design aspects of a 30-m Giant Infrared and Submillimeter Observatory in space ("GISMO"): a new "flavor" for SAFIR?. *Opt. Infrared, Millim. Space Telesc. Oct.* 9143, 1054–1065. doi:10.1117/12.551300

Hong, D., Gao, L., Yokoya, N., Yao, J., Chanussot, J., Du, Q., et al. (2020). More diverse means better: multimodal deep learning meets remote-sensing imagery classification. *IEEE Trans. Geoscience Remote Sens.* 59, 4340–4354. doi:10.1109/tgrs.2020.3016820

Hyde, R. A. (1999). Eyeglass. 1. Very large aperture diffractive telescopes. *Appl. Optics* 38, 4198–4212. doi:10.1364/ao.38.004198

Jian, Z., Mengjuan, L., Ganghua, Y., Jiao Jian-chao, 焦., Liu Zheng-kun, 刘., Xu Xiang-dong, 徐., et al. (2016). Large-diameter membrane Frensnel diffraction elements for space Telescope. *Opt. Precis. Eng.* 24, 1289–1296. doi:10.3788/ope.20162406.1289

Jiang, S., Zhi, X., Dong, Y., Zhang, W., and Wang, D. (2020). "Inversion restoration for space diffractive membrane imaging system,", 125. *Opt. Lasers Eng.* doi:10.1016/j.optlaseng.2019.105863

Kennedy, J., and Eberhart, R. (1995). Particle swarm optimization. *Proc. ICNN'95-international Conference Neural Networks* 4, 1942–1948. doi:10.1109/ICNN.1995.488968

Krishnan, D., and Fergus, R. (2009). Fast image deconvolution using hyper-laplacian priors. *Adv. Neural Information Processing Systems* 22. doi:10.5555/2984093.2984210

Kupyn, O., Martyniuk, T., Wu, J., and Wang, Z. (2019). *Deblurgan-v2: deblurring (orders-of-magnitude) faster and better paper presented at the International Conf.on Computer Vision 2019*. Seoul, Korea.

Li, J., Wen, L., Liu, H., Wei, G., Cheng, X., Li, Q., et al. (2023). A novel SPGD algorithm for wavefront sensorless adaptive optics system. *IEEE Photonics J.* 15, 1–9. doi:10.1109/jphot.2023.3285871

Li, J., Can, L., Zhengcong, D., Xiang, C., Qing, L., Lianghua, W., et al. (2025). A model-based image restoration method for diffraction imaging systems. *ACTA PHOTONICA SIN.* 54. doi:10.3788/gzxb20255402.0211002

Liang, W., Long, J., Li, K.-C., Xu, J., Ma, N., and Lei, X. (2021). A fast defogging image recognition algorithm based on bilateral hybrid filtering. *ACM Transactions Multimedia Computing, Communications, Applications (TOMM).* 17, 1–16. doi:10.1145/3391297

Lianghua, W., Yang, P., Kangjian, Y., Shanqiu, C., Shuai, W., Wenjing, L., et al. (2017). Synchronous model-based approach for wavefront sensorless adaptive optics system. *Opt. Express* 25, 20584–20597. doi:10.1364/OE.25.020584

Lianghua, W., Yang, P., Shuai, W., Wenjing, L., Shanqiu, C., and Xu, B. (2018). A high speed model-based approach for wavefront sensorless adaptive optics systems. *Opt. and Laser Technol.* 99, 124–132. doi:10.1016/j.optlastec.2017.08.022

Liping, H. Y., and Zhang, S. H. (2003). "A new approach to improve particle swarm optimization,", 2723. *Genet. Evol. Comput.* 134–139. doi:10.1007/3-540-45105-6_12

Lu, J., Qiao, K., Li, X., Lu, Z., and Zou, Y. (2019). Minimization methods for image restoration problems based on wavelet frames. *Inverse Probl.* 35, 064001. doi:10.1088/1361-6420/ab08de

Ruoqiu, W., Zhiyu, Z., and Donglin, X. (2017). Thin film fresnel diffractive elements with large aperture and high diffractive efficiency for space telescopes. *Infrared Laser Eng.* 46, 123–130. doi:10.3788/IRLA201746.0920001

Wang, Z.-Q., Zhang, H.-J., Fu, R.-L., Mu, G.-G., Lu, Z.-W., Cartwright, C. M., et al. (2002). Hybrid diffractive-refractive ultra-wide-angle eyepieces. *Optik* 113, 159–162. doi:10.1078/0030-4026-00134

Wang, L., Wu, S., and Yang, W. (2016). Mirror misalignment analysis of spliced Fresnel mirror. *Acta Opt. Sin.* 36, 0712002.

Wen, L., Huang, Q., and Xu, X. (2019). Adaptive optical optimization correction algorithm based on wavefront gradient squared. *Adv. Lasers and Optoelectron.* 56, 240103. doi:10.3788/L0P56.240103

Wen, L., Li, J., Du, Z., Li, Q., Cheng, X., Zhang, W., et al. (2024). "A novel image restoration approach based on model for Fresnel zone plate imaging system," in *Paper presented at the 2024 IEEE 4th international conference on information technology, big data and artificial intelligence (ICIBA)*.

Yang, J., Wang, S., Wen, L., Yang, P., Yang, W., Guan, C., et al. (2019). Experimental study on imaging and image deconvolution of a diffractive telescope system. *Appl. Opt.* 58, 9059–9068. doi:10.1364/AO.58.009059

Yang, J., Wang, S., Wen, L., Yang Ping, 杨., Yang Wei, 杨., Guan Chunlin, 官., et al. (2020). Faint-object imaging of diffractive telescopes based on image restoration. *Acta Opt. Sin.* 40, 1411005. doi:10.3788/aos202040.1411005

Zamir, S. W., Arora, A., Khan, S., Hayat, M., Khan, F. S., Yang, M.-H., et al. (2021). "Multi-stage progressive image restoration Paper presented at the 2021," in *IEEE/CVF conference on computer vision and pattern recognition (CVPR), Nashville, TN, USA, 20–25 June,2021*.

Zhang, N., Lu, Z., and Li, F. (2007). Optical design of diffractive telescope. *Infrared Laser Eng.* 36, 106. doi:10.3969/j.issn.1007-2276.2007.01.026

Zhi, X., Jiang, S., Zhang, W., Wang, D., and Li, Y. (2017). Image degradation characteristics and restoration based on regularization for diffractive imaging. *Infrared Phys. and Technol.* 86, 226–238. doi:10.1016/j.infrared.2017.09.014

Zhu, L., Wen, L., Yang, P., Guo, Z., Yang, W., Xu, B., et al. (2019). Aberration correction based on wavefront sensorless adaptive optics in membrane diffractive optical telescope. *Opt. Commun.* 451, 220–225. doi:10.1016/j.optcom.2019.06.063